Zhong, J., Yi, M., and Bau, H., H., 2002, A Magneto-Hydrodynamics (MHD) Pump Fabricated with Ceramic Tapes, Sensors and Actuators A Physical, 96, 1, 59-66.

MAGNETO-HYDRODYNAMIC (MHD) PUMP FABRICATED WITH CERAMIC TAPES

Jihua Zhong, Mingqiang Yi, Haim H. Bau
Department of Mechanical Engineering and Applied Mechanics
University of Pennsylvania, Philadelphia, PA 19104-6315, USA
e-mail: bau@seas.upenn.edu Fax: 215-573-6334

ABSTRACT

The use of Magneto Hydro Dynamics (MHD) to circulate fluids in conduits fabricated with low temperature co-fired ceramic tapes is described. Conduits shaped like toroidal and rectangular loops were fabricated. Electrodes printed on the ceramic substrate along the conduits' walls facilitated transmission of electric currents through the test fluids. When the devices were subjected to a magnetic field, the resulting Lorentz forces propelled the liquids. The paper details the fabrication process and describes experiments with mercury slugs, saline solution, and deionized water. The measured fluid velocities were compared with theoretical predictions.

Keywords: Microfluidic devices, Magneto Hydro Dynamics, MHD, pump

1. INTRODUCTION

In recent years, there has been a growing interest in developing minute chemical and biological laboratories and reactors. Often it is necessary to propel fluids from one part of a device to another, control the fluid motion, mix, and separate fluids. In microdevices, these tasks are far from trivial. Typically, electrostatic forces are being used to move liquids around. These forces usually induce only very low flow rates, require the use of high electrical potentials, and may cause significant heating of the solution. The use of electromagnetic forces presents an interesting, flexible means for manipulating liquids in micro fluidic devices and systems. The only requirement is that the liquid be at least slightly conductive. This requirement is met by many biological solutions.

The application of electromagnetic forces to pump, confine, and control fluids is not new. The field is generally known as Magneto Hydro Dynamics (MHD), and it deals with the conversion of electromagnetic energy into mechanical work in fluid media [1,2]. To date, MHD has mostly been used to pump and control highly conducting fluids such as liquid metals and ionized gases and to study ionospheric/astrophysical plasmas. MHD models are also extensively used in the analysis of magnetic fusion devices. The potential use of electromagnetic forces in

microdevices has attracted much less attention. Recently, a few researchers [3,4] constructed MHD micro-pumps on a silicon substrate and demonstrated that these pumps are able to move liquids around in micro conduits. MHD can be used not only for the purpose of pumping fluids but also to induce secondary complex flows that may be beneficial for stirring and mixing [5, 6, 7]. Furthermore, by patterning electrodes in a desired fashion, one can propel liquids in virtual, wall-less channels. In this paper, we describe the fabrication of MHD pumps with low temperature, co-fired ceramic tapes.

We start by briefly reviewing the theory of MHD pumping. We then describe two MHD pumps fabricated with low temperature ceramic tapes. Although MHD pumps can be fabricated in various substrate materials, ceramic tapes offer a particularly convenient substrate medium by being highly dielectric and by being a layered manufacturing technology that facilitates integration of hydraulic conduits and metallic paths in a three-dimensional setting. Finally, we describe a few experiments in which we propelled mercury slugs, saline solution, and deionized water in toroidal and rectangular planar "loops." The experimental measurements are compared with theoretical predictions.

2. THEORY

In this section, we review briefly the fundamental principles of MHD pumping. Consider a nearly straight conduit of length (L) with a rectangular cross-section of height H and width W aligned in the x_2-x_3 plane (Fig. 1). The coordinate x_1 is directed along the conduit's axis. Perfectly conducting electrodes are deposited on the two opposite sides of the conduit. The conduit is filled with a liquid of electrical conductivity σ and viscosity μ. The liquid needs to be only slightly conductive. The electrodes are subjected to a potential difference (V) that induces a current of density $\mathbf{J} = J\hat{e}_3$. The conduit is relatively long; fringe effects are neglected, and the current flow is assumed to be one-dimensional. The conduit is placed in a magnetic field of flux density $\mathbf{B} = B\hat{e}_2$ directed in the x_2-direction.

Ohm's law for a moving conductor of conductivity σ in a magnetic field is

$$\mathbf{J} = \hat{e}_3\sigma\left(E + vB\right), \tag{1}$$

where $\hat{e}_i$ and $v(x_2,x_3)$ are, respectively, a unit vector in the (i) direction and the fluid's velocity component in the x_3-direction. E is the electric field. The interaction between the electric current and the magnetic field generates a

Lorentz force of density $\mathbf{J}\times\mathbf{B}$ in the x_1-direction. We assume that the electrodes are relatively long, L>>W, and the fluid flow is fully developed ($\frac{\partial}{\partial x_1}=0$). The dimensionless, time-independent Navier-Stokes equation for an incompressible, fully developed flow in a straight conduit is:

$$\left(\frac{\partial^2}{\partial x_2^2}+\frac{\partial^2}{\partial x_3^2}\right)v - Ha^2 v = 1 \quad (0<x_2<1,\ 0<x_3<\alpha) \tag{2}$$

In the above, we use the conduit width, W, as the length scale and $\left|\frac{\sigma VBW}{\mu}\right|$ as the velocity scale. The axial velocity, $v(x_2,x_3)$, satisfies no-slip conditions at all solid walls: $v(0,x_3)=v(W,x_3)=v(x_2,0)=v(x_2,H)=0$. $Ha = BW\sqrt{\frac{\sigma}{\mu}}$ is the Hartman number. α=H/W is the conduit's aspect ratio. When the liquid is a poor conductor of electricity such as saline solution, Ha<<1 and the second term in equation (2) can be safely neglected. When the liquid is metal such as mercury, the Hartman number may be on the order of 10, and the second term in (2) must be accounted for.

The above analysis indicates that the fluid velocity is proportional to the characteristic length (W). In microfluidic systems, where W is small, this compares unfavorably with electro-osmotic flows in which the velocity scales like $\frac{\varepsilon\zeta}{\mu}\left(\frac{V}{L}\right)$, where L is the conduit's length, ζ is the electrokinetic (zeta) potential, and ε is the permittivity. Nevertheless, MHD has a fair amount of advantages. The magnetic field can be applied externally so that B can be fairly large. Long conduits with electrodes can be used to achieve high pressures. Moreover, the electrodes can be printed at the bottom of the conduit in a complex pattern leading to intricate flow fields. Finally, by manipulating the directions of the electric and magnetic fields, one can generate flow fields with both spatial and temporal complexity.

With Mathematica's [8] assistance, equation (2) can be readily solved using the Fourier series expansion:

$$v(x_2,x_3) = -\frac{4}{\pi}\sum_{n=1}^{\infty}\frac{1}{1+2n}\left(1-\frac{\cosh\left(\lambda_n\left(\frac{\alpha}{2}-x_2\right)\right)}{\cosh\left(\lambda_n\frac{\alpha}{2}\right)}\right)\sin\left((2n+1)\pi x_3\right), \tag{3}$$

where $\lambda_n^2 = Ha^2 + (2n+1)^2\pi^2$. When Ha=0, expression (3) is identical to that of pressure-driven Poiseuille flow in a conduit with a rectangular cross-section (i.e., White [9], page 123). Indeed, when the Hartman number is small, the Lorentz force plays a similar role to that of the pressure gradient.

By integrating (3) over the cross-sectional area, we obtain the flow rate in the conduit:

$$Q = \frac{8}{\pi^2}\sum_{n=1}^{\infty}\frac{1}{(1+2n)^2\lambda_n^2}\left(1-\frac{2}{\lambda_n\alpha}\tanh(\lambda_n\frac{\alpha}{2})\right). \quad (4)$$

When the Hartman number is small, series (3) and (4) converge rapidly. The convergence rate deteriorates as the Hartman number increases. For large Hartman numbers, one can work out asymptotic approximations for the velocity field and the flow rate. Since here we are interested only in low and moderate Hartman numbers, expressions (3) and (4) will suffice for our purposes.

When α=1, Fig. 2 depicts the velocity profile at the cross-section's mid-height, $|v(x_2,0.5)|$, as a function of x when Ha=0 and Ha=10. When Ha>0, the velocity profile is parabolic just as in the case of pressure-driven Poiseuille flow. As the Hartman number increases, the maximum velocity declines and the velocity profile flattens. In order to accommodate conveniently both velocity profiles on the same graph, we multiplied the velocity for Ha=10 by the factor 7.

When α=1, Fig. 3 depicts the centerline velocity (upper curve) |v(0.5,0,5)| and the flow rate Q (lower curve) as functions of the Hartman number. As the Hartman number increases, the maximum velocity and the flow rate decrease. The flow rate decreases at a somewhat slower pace than the rate of decrease of the maximum velocity. This is because of the flattening of the velocity profile as the Hartman number increases, as is evident in Fig. 2. In other words, as the Hartman number increases, |v(0.5,0.5)|->Q.

2. FABRICATION

We constructed the prototypes of the MHD pumps with low temperature, co-fired ceramic tapes (LTCC). LTCC technology facilitates inexpensive, rapid prototyping, and provides a rapid platform for the integration of passive electronics and fluidics.

In their pre-fired (green) state, the ceramic tapes consist of oxide particles (i.e., alumina), glass frit, and organic binder (that can be made from photo-resist). The tapes are typically available at thicknesses starting at 100μm±7%.

One can cast, however, even thinner tapes. In the pre-fired state, the tapes can be machined by laser, milling, and photolithography (when the binder is photo-resist). Metallic paths can be either printed or processed photolithographically to form electrodes, resistors, conductors, and thermistors. Conduit sizes may range from ~10μm to a few millimeters. Upon firing, the organic binder burns out, the oxide particles sinter, and the tapes solidify. Many tapes (>80) can be stacked together, aligned, laminated, and co-fired to form monolithic structures with complex, three-dimensional mazes of fluidic conduits, electronic circuits, and electrodes. Glass windows and other materials can be readily attached to the tapes to facilitate optical paths. Multiple layers of coils can be embedded in the tapes to generate magnetic fields [10, 11]. As the application of LTCC for the fabrication of fluidic systems is relatively new, there is little experience with respect to the reproducibility of the machined features. We estimate that one can achieve reproducibility within 5%.

Two different crude prototypes of MHD pumps were fabricated with DuPont, LTCC 951AT tapes that have nominal (pre-fired) thicknesses of ~125μm and ~250μm. One prototype housed the toroidal conduit (Fig. 4) and the other a rectangular loop (Fig. 5). The toroidal conduit that was used in the experiments with mercury was 22mm in inner diameter, 2.2mm wide, and 700μm deep. The toroidal conduit that was used in the water experiments was 1.4mm wide and 700μm deep. The inner part of the rectangular loop was 13.5mm long and 6.7mm high, and the conduit's width and height were, respectively, 1.2mm and 700μm.

The fabrication process consisted of blanking rectangular segments of tapes to a desired size. The various layers were machined individually using a numerically controlled milling machine. Subsequently, electrodes and conductor paths were printed on the various layers. Fig. 6 depicts schematically the various layers that were used in the fabrication of the toroidal loop and the features that were machined on them. The layer numbers should be cross-referenced with the cross-sectional view shown in Fig. 4b. The rectangular loop was constructed in a similar way.

In Fig. 6, the circular hole machined in layer 1 provided a cavity for housing the permanent magnet. Layer 2 includes a conductor path (the dark line, DuPont 5734 gold paste) that facilitates the connection of the inner electrode to a power supply. The two circular electrodes were made with 20μm thick DuPont 5734 gold paste and printed on layer 3. The straight conductor segments connected the electrodes to the location of the vias. A few layers of type 4 were used to form the conduit. These layers also housed vertical vias. The number of layers of type 4 determined the height of the conduit. Layer 5 forms the cover (which we did not use in our experiments so as to enable flow visualization). The vias were filled with silver paste (DuPont 6141) and terminated with soldering pads

(DuPont 6146) on the top surface. Subsequent to the machining and printing, the layers were stacked, aligned, laminated, and co-fired to form a monolithic block.

The cross-section of the assembled device is shown schematically in Fig. 4b. In our experiments, we positioned, respectively, a circular, permanent Neodymium (NdFeB) magnet (Edmund Scientific, serial number CR35-107, load carrying capacity of 15 lb, 1" diameter and 0.25" height) and two rectangular magnets bounded together (Edmund Scientific, serial number CR81-237, load-carrying capacity of 12-15 lb, 32mm × 16.76mm × 9.91mm) under the toroidal and rectangular loops. The magnetic field can also be generated by other means. For example, one can machine the conduits in magnetic tapes. Alternatively, one can use an external electromagnet or coils embedded in the ceramic tapes [12]. In the latter case, soft magnetic material such as permalloy can also be encapsulated in the tapes to focus the magnetic field. In order to allow the transmission of significant electric currents through the electrolyte without bubble generation and to prevent electrode degradation (which turned out to be a serious problem in our experiments), it would be preferable to use an AC current. By appropriate synchronization of the electromagnetic field with the AC current, the direction of the Lorentz force would remain unaltered [4].

4. EXPERIMENTS

We carried out experiments both in the toroidal and the rectangular loops with mercury slugs, deionized water, and saline solution. Power was supplied to the electrodes using an adjustable power supply (HP 6032A). The power supply also provided current data with a resolution of about 10mA that turned out to be insufficient for most of our needs.

4.1 Experiments with Mercury

Experiments were carried out in both open and capped conduits. In the latter case, the conduit was capped with a glass slide after the introduction of the mercury slug into the conduit. A mercury slug of an approximate length of 4mm was inserted in the conduit. In the presence of the slug, the total electric resistance of the system (including contact resistances) both in the uncapped and capped conduits was 0.2ohm. The effective conductivity of the mercury was estimated to be $\sigma=10^6(\Omega\bullet m)^{-1}$. The voltage differential across the electrodes was gradually increased. When the voltage increased very slowly, once it exceeded a certain value, the slug deformed and "splashed" along

the inner electrode. When the voltage was increased at a sufficiently rapid rate, once it exceeded a threshold, V_1, the mercury slug started moving around the toroidal conduit. The threshold voltages for the open and closed conduits were, respectively, V_1=0.35 and V_1=0.5V. The slug's motion was monitored with a video camera. During its motion, the slug appeared to elongate to about 5.3mm, apparently at the expense of its height.

Figs. 7 and 8 depict, respectively, the slug's velocity as a function of the applied voltage in the open and capped conduits. In the open and capped conduits, the voltage ranged, respectively, up to 0.4V and 0.9 V. The symbols, solid line, and dashed line correspond, respectively, to experimental data, theoretical predictions for the maximum velocity, and theoretical predictions for the average velocity. The difference between the average and maximum velocities is relatively small since the Hartman number is larger than 10 (see Fig. 3). The slug's velocity was measured by counting the number of revolutions that the slug completed within a given amount of time. The vertical bars indicate the estimate of the experimental error.

The experiment was carried out by gradually increasing the voltage. Motion was observed once $V>V_1$, and in the range tested, the slug speed increased nearly linearly as the voltage was further increased, i.e., the measured speed can be correlated with $v \sim a*V$. In the open and capped conduits, $a \sim 0.59$ m/s/V and ~0.19 m/s/V, respectively. Not surprisingly, due to the additional friction, the slug's velocity in the capped conduit was lower than in the open conduit. Eventually, once motion was established, we decreased the voltage gradually. As the voltage decreased so did the speed of the slug. When $V>V_1$, the velocities when the voltage was decreased were about the same as when the voltage was increased. The slug kept moving, however, at voltages smaller than the threshold voltage for the onset of motion, V_1. Once the voltage was reduced below a second threshold, $0<V_2<V_1$, the slug came to a stop. In the open and capped conduits, V_2=0.17 and 0.20V, respectively. In other words, the slug exhibited a hysteresis phenomenon. In the voltage range $V_2<V<V_1$, motion was sustained only when the slug started from a motion state. We suspect that this hysteresis was predominantly caused by static friction. The lack of motion when $V<V_1$ is probably due to contact resistance.

We conducted experiments up to velocities of 0.2m/s. That is, the slug completed a full circle in less than one second. We did not go to higher speeds out of fear that centrifugal forces would project the slug out of the uncapped conduit and because it became increasingly difficult to monitor the slug's velocity. By reversing the electrode's polarity, the slug's direction of motion was reversed. The mercury slug required a fair amount of power to propel.

Fig. 9 depicts the slug's velocity in the uncapped, toroidal loop as a function of the power consumption expressed in Watts.

A second set of experiments with a mercury slug was conducted in the rectangular channel. We inserted a mercury slug in the conduit section containing the parallel electrodes and applied low frequency (<100Hz), alternating voltage to the electrodes. As a result, the Lorentz force changed direction, causing the mercury slug to exhibit linear, oscillatory motion.

4.2 WATER AND SALINE SOLUTION

We carried out experiments with de-ionized water and saline solutions. The resistance of the entire system was measured at the onset of the experiments, and the specific apparent conductivity was determined to be, respectively, $\sigma = 2.2\times10^{-4}\ (\Omega\bullet m)^{-1}$ and $\sigma = 2.2\times10^{-3}\ (\Omega\bullet m)^{-1}$ for the de-ionized water and saline solutions. The experiment was complicated by the gradual dissolution of the electrodes that resulted in the gradual increase in the solutions' conductivity. The life expectancy of the electrodes depends, among other things, on the paste material, the thickness of the thick film, and the current's intensity. The electrodes made out of gold paste lasted typically for about one hour of operation. This undesirable deterioration of the electrodes as well as bubble generation can be eliminated through the use of alternating currents and magnetic fields [4]. However, this remedy was not attempted here.

In all cases, the Hartman number was very small, and its effects could be safely ignored. Experiments were conducted both in the toroidal and rectangular loops. In the toroidal loop containing saline solution, we monitored the liquid speed by tracking a small particle suspended in the liquid. Because of the relatively high velocities that were achieved by the saline solution in the toroidal loop, tracking the fluid velocity with a dye was impractical. In the cases of the toroidal loop operating with de-ionized water and the rectangular conduit operating with both de-ionized water and saline solutions, the velocities were much lower and were monitored by tracking a dye. The saline solution in the rectangular loop was slower than in the toroidal loop because only one leg of the rectangular loop was actuated. To account for the effects of diffusion, we employed two different strategies. In the first strategy, once the drop of dye was injected into the test liquid, we monitored as a function of time the progression of both the dye's leading and trailing edges and then estimated the velocity of the colored blob's center. In the second strategy, we injected a drop of dye into the conduit in the absence of an electric field. When the liquid was stationary, we monitored the spreading of the dye due to diffusion alone as a function of time. This allowed us to

estimate the progression of the leading and trailing edges due to diffusion. This data was later subtracted from the monitored locations of the leading and trailing edges at corresponding times and in the presence of fluid motion. Both methods yielded essentially identical results.

Figs. 10 and 11depict, respectively, the velocity (mm/s) of the de-ionized water and saline solutions in the toroidal loop as functions of the applied voltage. The current's magnitude was estimated to be in the μA range and well below the measurement capabilities of our power supply. The symbols, solid line, and dashed line correspond, respectively, to the measured velocity, the predicted maximum velocity, and the predicted average velocity.

For the construction of Fig. 10, we monitored the electric conductivity of the solution throughout the experiment. In other words, the electric conductivity of the liquid varied from one data point to another. In Fig. 11, we used the electric conductivity at the beginning of the experiment.

Fig. 12 depicts, as a function of the applied voltage, the velocity (mm/s) of the saline solution in the rectangular loop. The symbols, solid line, and dashed line correspond, respectively, to the measured velocity, the predicted maximum velocity, and the predicted average velocity. Here again, the electric conductivity was measured only at the beginning of the experiment.

The data is in qualitative agreement with theoretical predictions. Given the significant differences between the mathematical model and the physical set-up, perfect agreement could not be expected. The mathematical model assumed uniform current density. In contrast, in the experiment, the electrodes were printed along the conduit's bottom resulting in more complex current distribution. The comparison between theory and experiment was also complicated by the fact that we did not have accurate knowledge of the magnetic field and by the continuous deterioration of the electrodes.

CONCLUSIONS

The paper demonstrates that magnetic forces can be utilized to propel liquids such as mercury, saline solution, and de-ionized water in minute conduits. Experimental observations were in qualitative agreement with theoretical predictions. Low temperature, co-fired ceramic tapes provide a particularly convenient platform for the construction of MHD devices because they allow the integration of electrodes, conductors, and hydraulic paths in the pre-fired, green state. The technology also facilitates the construction of three-dimensional structures, all of which can be served by the same magnetic field. The LTCC technology allows one to integrate multiple layers of

coils into the substrate for the generation of the magnetic fields. Coils can also be conveniently embedded around the conduits to monitor the flow rates in-situ. Finally, one can use magnetic tapes to provide the necessary magnetic field.

The pressure head generated by the MHD pump can be controlled by adjusting the intensity of the magnetic field, the magnitude of the applied voltage across the electrodes, and the length of the actuated section. By using a great length of meandering conduits, it is possible to achieve considerable pressure heads. The magnetic forces can be utilized not only for pumping purposes but also to induce the complex flow patterns needed to stir the fluid and enhance mixing [5, 6, 7]. Moreover, one can use MHD to control fluid flow in a fluidic network very much in the same way as one would control current flow in an electrical network and without the need for valves and pumps [6]. To this end, one would deposit parallel electrodes along each of the network's legs (conduits) in the same way as we described in this paper. By controlling the voltage across each electrode pair, one can direct the fluid flow in any desired way. By reversing the electrodes' polarity, the direction of the flow will be reversed.

During the experiments, our devices suffered from the gradual deterioration of the electrodes. This may not be a problem in devices that are meant to operate for only short amounts of time. In any event, this problem can be reduced by proper choice of materials and possibly eliminated altogether by employing an AC potential with appropriately synchronized alternating direction magnetic field as was suggested by Lemoff and Lee [4].

ACKNOWLEDGMENTS

The work described in this paper was supported, in part, by DARPA through grant N66001-97-1-8911 to the University of Pennsylvania. DuPont has supplied us freely with materials.

REFERENCES

1. H. H. Woodson and J. R. Melcher, 1969, Electromechanical Dynamics, Vol. III, John Wiley.
2. P. A. Davidson, An Introduction to Magnetohydrodynamics, Cambridge 2001
3. J. Jang and S. S. Lee, 2000, Theoretical and Experimental Study of MHD (Magnetohydrodynamic) Micropump, Sensors and Actuators A, 80, 84-89.
4. A. V. Lemoff and A. P. Lee, 2000, An AC Magnetohydrodynamic Micropump, Sensors and Actuators B, 63, 178-185.

Zhong, J., Yi, M., and Bau, H., H., 2002, A Magneto-Hydrodynamics (MHD) Pump Fabricated with Ceramic Tapes, Sensors and Actuators A Physical, 96, 1, 59-66.

5. H. H. Bau, J. Zhong and M. Yi, 2001, A Minute Magneto Hydro Dynamic (MHD) Mixer, to appear in Sensors and Actuators B.
6. H. H. Bau, 2001, A Case for Magnetohydrodynamics, Proceedings of the 2001 ASME International Mechanical Engineering Congress and Exhibition, New York, NY 2001.
7. M. Yi and H. H. Bau, A Magneto-hydrodynamic (MHD) Chaotic Stirrer, submitted to J. Fluid Mechanics.
8. S. Wolfram, 1996, Mathematica, Cambridge.
9. F. M. White, 1974, Viscous Fluid Flow, McGraw Hill
10. H. H. Bau, G. K. Ananthasuresh, J. J. Santiago-Aviles, J. Zhong, M. Kim, M. Yi, and P. Espinoza-Vallejos, 1998, Ceramic Tape-Based Systems Technology, Micro-Electro-Mechanical Systems (MEMS), DSC-Vol. 66, 491-498.
11. M. Kim, M. Yi, J. Zhong, H. H. Bau, H. Hu, and G. K. Ananthasuresh, 1998, The Fabrication of Flow Conduits in Ceramic Tapes and the Measurement of Fluid Flow Through These Conduits. Micro-Electro-Mechanical Systems (MEMS), DSC-Vol. 66, 171-177.
12. M. Gongora-Rubio, J. J. Santiago-Aviles, L. Sola-Laguna, L., and M. Smith, 1999, Integrated LTCC Coils for Multiple Applications in Meso Electro Mechanical Systems, ASME: Micro-Electro-Mechanical Systems (MEMS 1), Nashville TN, 189-194.

LIST OF CAPTIONS

1. Conduit's cross-section
2. The velocity profiles, $|v(x_2,0.5)|$ and $7|v(x_2,0.5)|$, are depicted as functions of x when Ha=0 and Ha=10, respectively. Conduit aspect ratio, α=1.
3. The centerline velocity and the flow rate are depicted as functions of the Hartman number (Ha). Conduit aspect ratio, α=1.
4. A top view photograph of the toroidal conduit fabricated with low temperature ceramic tapes. (b) A cross-section (not drawn to scale) of the toroidal loop. The various layers' numbers are cross-referenced with Fig. 6.
5. A rectangular loop fabricated in LTCCs. Electrodes were printed only along the upper conduit.
6. The various LTCC layers that were used in the construction of the toroidal pump. Layer 1 houses the permanent magnet. Layer 2 supports a conductor. Layer 3 houses the electrodes and provides the bottom wall of the conduit. Layer 4 houses the conduit. A few layers of type (4) are used to obtain the desired conduit height. Layer 5 (not used in our experiments) caps the conduit.
7. The velocity (cm/s) of the mercury slug in an uncapped, toroidal conduit as a function of the applied voltage. The symbols, solid line, and dashed line correspond, respectively, to experimental data, maximum theoretical velocity, and average theoretical velocity.
8. The velocity (cm/s) of the mercury slug in a capped, toroidal conduit as a function of the applied voltage. The symbols, solid line, and dashed line correspond, respectively, to experimental data, maximum theoretical velocity, and average theoretical velocity.
9. The mercury slug's velocity in the uncapped toroidal loop as a function of the power consumption.
10. The velocity is depicted as a function of the applied voltage for deionized water in a toroidal conduit. The symbols, solid line, and dashed line correspond, respectively, to the experimental data (approximately maximum velocity), the prediction for the maximum velocity, and the prediction for the average velocity. The calculations were carried out based on the electric conductivity at the beginning of the experiment.
11. The velocity is depicted as a function of the applied voltage for saline solution in a toroidal conduit. The symbols, solid line, and dashed line correspond, respectively, to the experimental data for approximately the maximum velocity, the prediction for the maximum velocity, and the prediction for the average velocity. The

electric conductivity was periodically measured, and theoretical predictions at various voltages correspond to different electric conductivities.

12. The velocity is depicted as a function of the applied voltage for saline water in the rectangular loop. The symbols, solid line, and dashed line correspond, respectively, to the experimental data for approximately the maximum velocity, the prediction for the maximum velocity, and the prediction for the average velocity. The electric conductivity was measured at the beginning of the experiment.

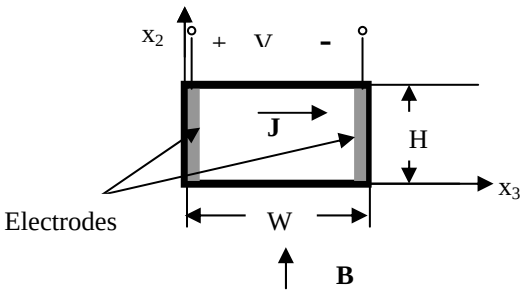

Fig. 1: Conduit's cross-section

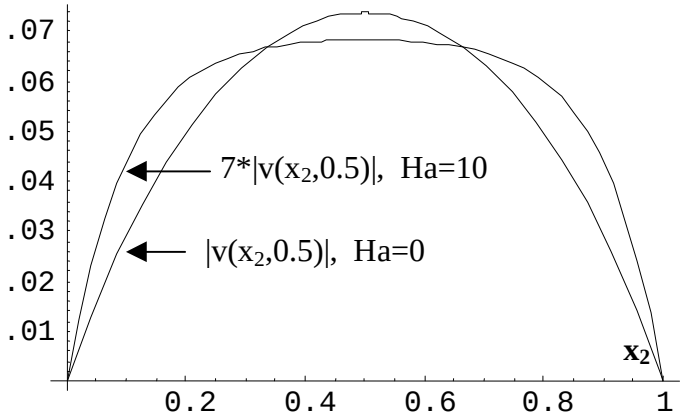

Fig. 2: The velocity profiles, $|v(x_2,0.5)|$ and $7|v(x_2,0.5)|$, are depicted as functions of x when Ha=0 and Ha=10, respectively. α=1.

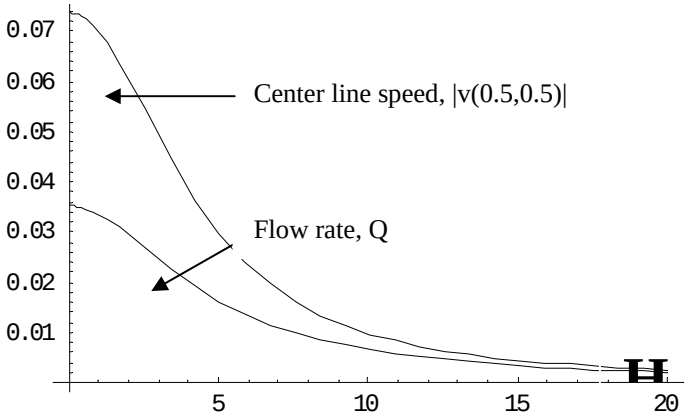

Fig. 3: The centerline velocity and the flow rate are depicted as functions of the Hartman number (Ha). α=1.

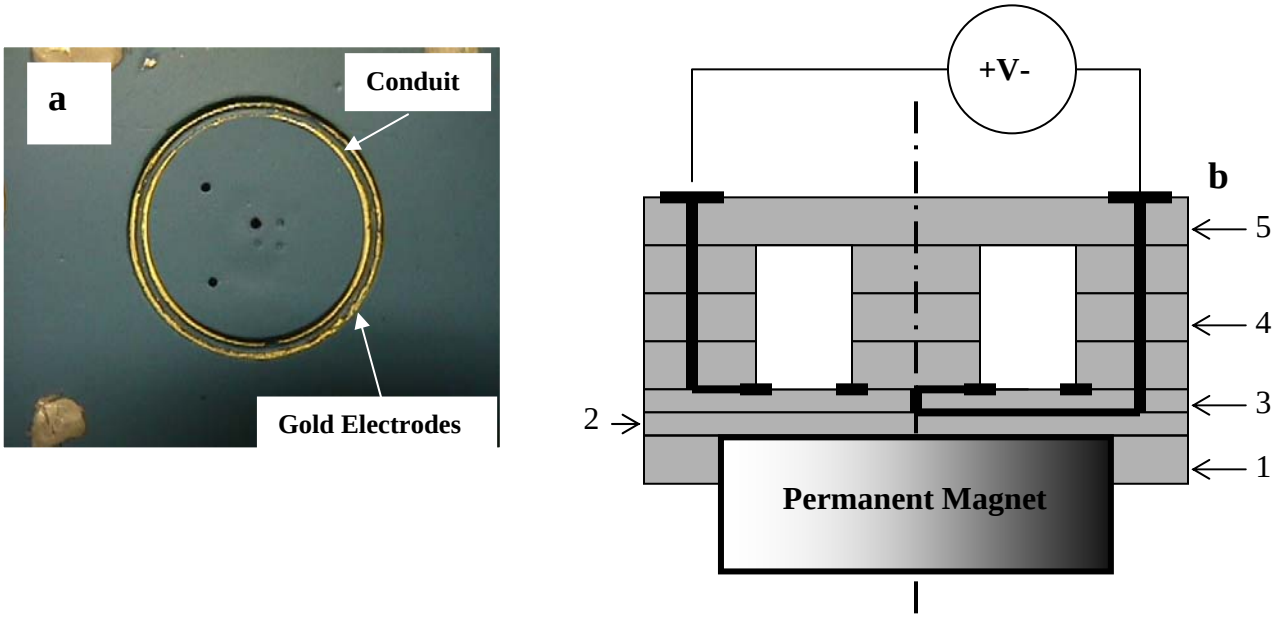

Fig. 4: (a) A top view photograph of the toroidal conduit fabricated with low temperature ceramic tapes. (b) A cross-section (not drawn to scale) of the toroidal loop. The various layers' numbers are cross-referenced with Fig. 6.

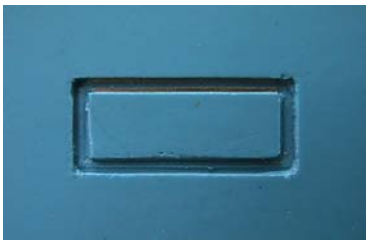

Fig. 5: A rectangular loop fabricated in LTCCs. Electrodes were printed only along the upper conduit.

Zhong, J., Yi, M., and Bau, H., H., 2002, A Magneto-Hydrodynamics (MHD) Pump Fabricated with Ceramic Tapes, Sensors and Actuators A Physical, 96, 1, 59-66.

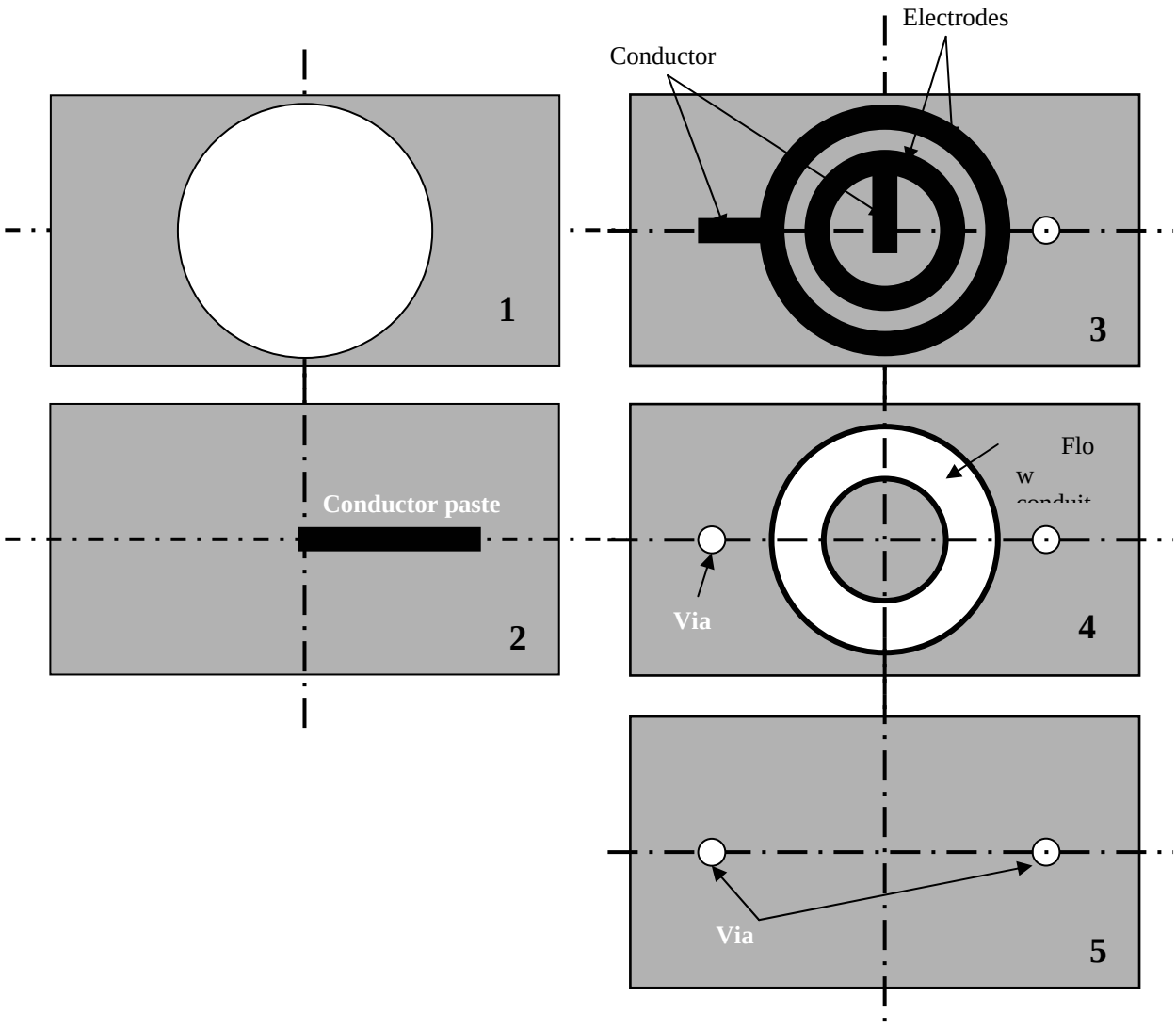

Fig. 6: The various LTCC layers that were used in the construction of the toroidal pump. Layer 1 houses the permanent magnet. Layer 2 supports a conductor. Layer 3 houses the electrodes and provides the bottom wall of the conduit. Layer 4 houses the conduit. A few layers of type 4 are used to obtain desired conduit height. Layer 5 (not used in our experiments) caps the conduit.

Zhong, J., Yi, M., and Bau, H., H., 2002, A Magneto-Hydrodynamics (MHD) Pump Fabricated with Ceramic Tapes, Sensors and Actuators A Physical, 96, 1, 59-66.

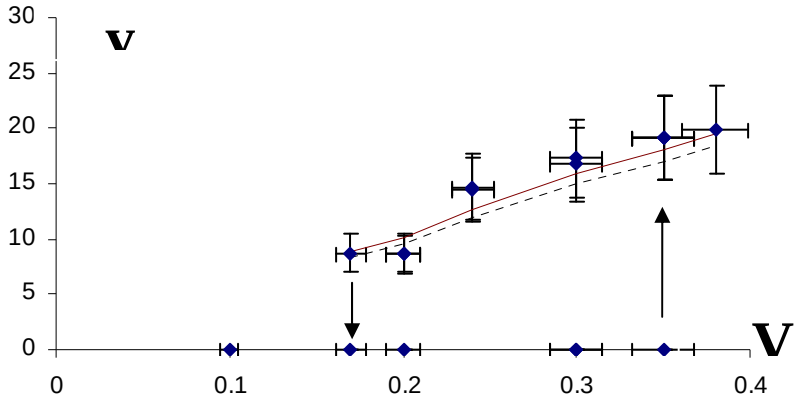

Fig. 7: The velocity (cm/s) of the mercury slug in an uncapped, toroidal conduit as a function of the applied voltage. The symbols, solid line, and dashed line correspond, respectively, to experimental data, maximum theoretical velocity, and average theoretical velocity.

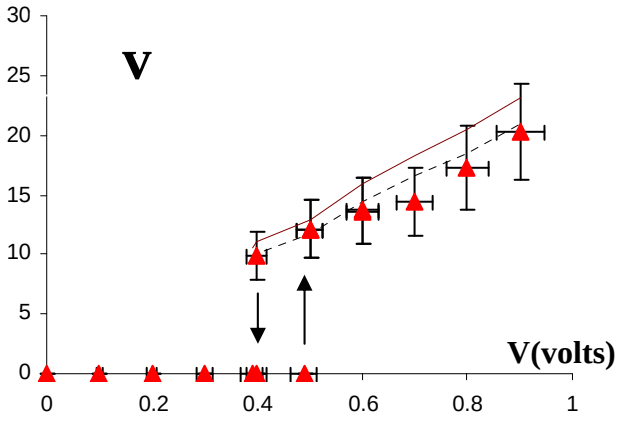

Fig. 8: The velocity (cm/s) of the mercury slug in a capped, toroidal conduit as a function of the applied voltage. The symbols, solid line, and dashed line correspond, respectively, to experimental data, maximum theoretical velocity, and average theoretical velocity.

Zhong, J., Yi, M., and Bau, H., H., 2002, A Magneto-Hydrodynamics (MHD) Pump Fabricated with Ceramic Tapes, Sensors and Actuators A Physical, 96, 1, 59-66.

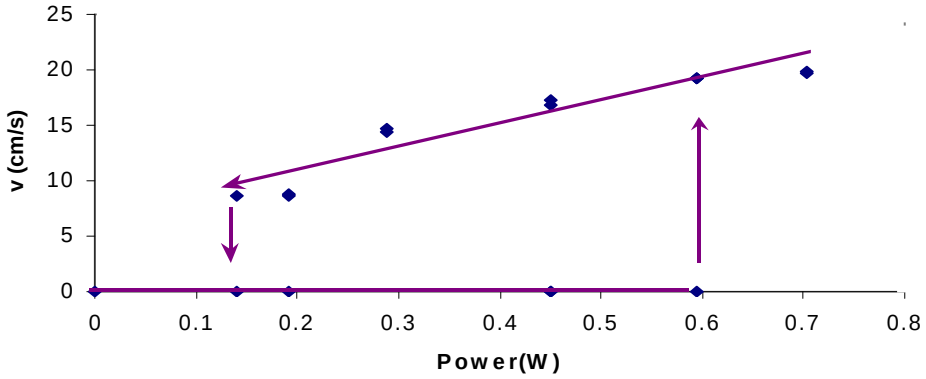

Fig. 9: The mercury slug's velocity in the uncapped toroidal loop as a function of the power consumption.

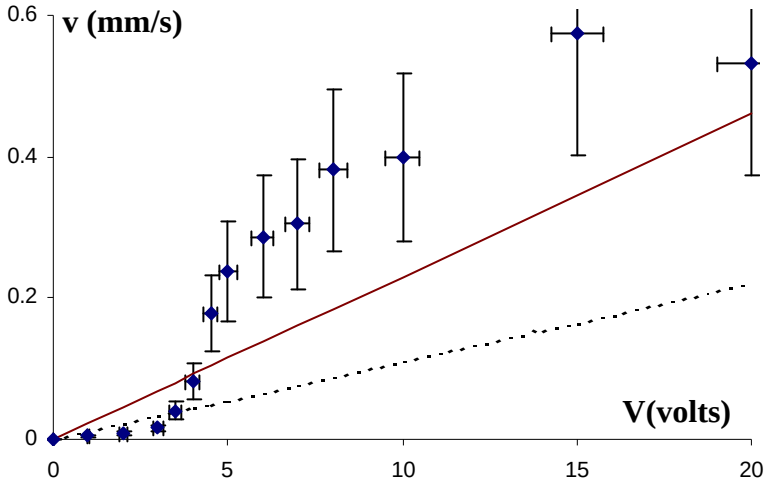

Fig. 10: The velocity is depicted as a function of the applied voltage for de-ionized water in a toroidal conduit. The symbols, solid line, and dashed line correspond, respectively, to the experimental data (approximately maximum velocity), the prediction for the maximum velocity, and the prediction for the average velocity. The calculations were carried out based on the electric conductivity at the beginning of the experiment.

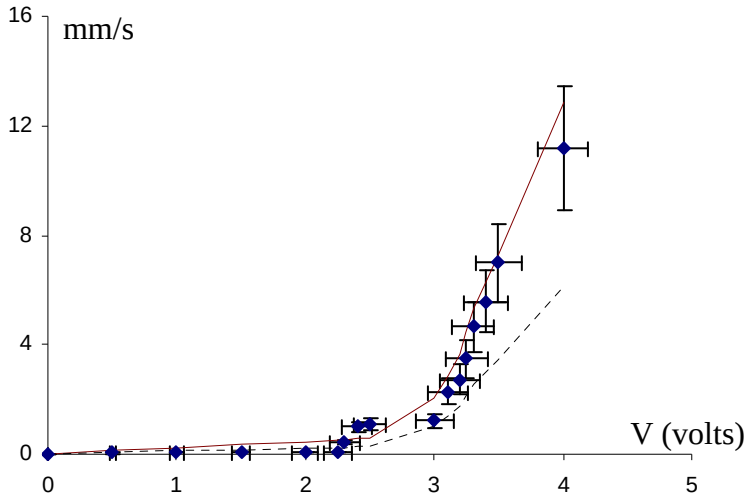

Fig. 11: The velocity is depicted as a function of the applied voltage for saline solution in a toroidal conduit. The symbols, solid line, and dashed line correspond, respectively, to the experimental data for approximately the maximum velocity, the prediction for the maximum velocity, and the prediction for the average velocity. The electric conductivity was periodically measured, and theoretical predictions at various voltages correspond to different conductivities.

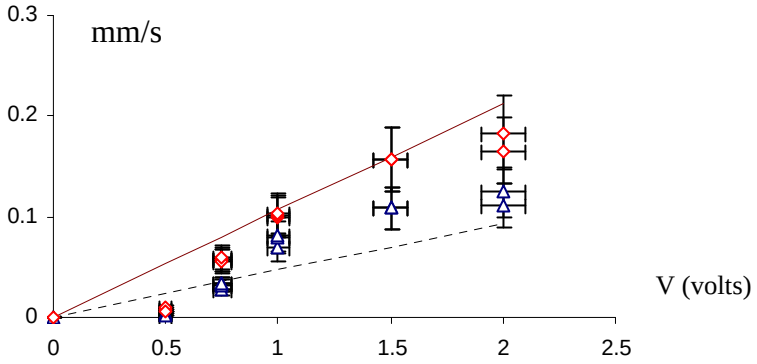

Fig. 12: The velocity is depicted as a function of the applied voltage for saline water in the rectangular loop. The symbols, solid line, and dashed line correspond, respectively, to the experimental data for approximately the maximum velocity, the prediction for the maximum velocity, and the prediction for the average velocity. The electric conductivity was measured at the beginning of the experiment.